applied sciences

MDPI

Article

Modeling and Evaluation of Reversible Traction Substations in DC Railway Systems: A Real-Time Simulation Platform Toward a Digital Twin

Dario Zaninelli *, Hamed Jafari Kaleybar * and Morris Brenna

Department of Energy, Politecnico di Milano, 20156 Milan, Italy; morris.brenna@polimi.it
* Correspondence: dario.zaninelli@polimi.it (D.Z.); hamed.jafari@polimi.it (H.J.K.)

Abstract

Traditional diode-based rectifiers (TDRs) in railway traction substations (TSSs) are inefficient at handling bidirectional power flow and cannot recover regenerative braking energy (RBE). Replacing these conventional systems with reversible traction substations (RTSSs) requires detailed modeling, extensive simulations, and validation using real data. This paper presents a DT-oriented real-time modeling and Hardware-in-the-Loop (HIL) platform for the analysis and performance assessment of RTSSs in DC railway systems. The integration of interleaved PWM rectifiers enables bidirectional power flow, allowing efficient RBE recovery and its return to the main grid. Modeling railway networks with moving trains is complex due to nonlinear dynamics arising from continuously varying positions, speeds, and accelerations. The proposed approach introduces an innovative multi-train simulation method combined with low-level transient and power-quality analysis. The validated DT model, supported by HIL emulation using OPAL-RT, accurately reproduces real-world system behavior, enabling optimal component sizing and evaluation of key performance indicators such as voltage ripple, total harmonic distortion, passive-component stress, and current imbalance. The results demonstrate improved energy efficiency, enhanced system design, and reduced operational costs. Meanwhile, experimental validation on a small-scale RTSS prototype, based on data from the Italian 3 kV DC railway system, confirms the accuracy and applicability of the proposed DT-oriented framework.

Keywords: railway systems; digital twin-oriented model; regenerative braking energy; harmonic; power quality; real-time

Academic Editor: Suchao Xie

Received: 28 October 2025
Revised: 8 December 2025
Accepted: 15 December 2025
Published: 21 December 2025

1. Introduction

Achieving zero-carbon transportation systems by 2050 would be a major step forward for the transportation industry and aligns with the commitments set forth by the EU's climate targets [1,2]. In this context, the EU Green Deal and the "Fit for 55" package explicitly emphasize the need to increase the share of electrified rail transport and to enhance the efficiency of existing railway infrastructure as key measures for reducing sector-wide emissions. These policies are accelerating the deployment of advanced electrified railway technologies capable of improving system-level energy performance, integrating renewable generation, and enabling flexible interaction with the public grid. As a result, creative approaches to enhancing energy efficiency in electric railway systems are gaining traction. Among these, the recovery and reuse of regenerative braking energy (RBE) has attracted significant attention, with numerous studies investigating its potential and associated

technological solutions [3–5]. Regenerative braking represents a major opportunity for improving the energy efficiency of DC railway systems, with studies reporting that up to 20% of traction energy can be theoretically recovered [6]. However, the actual recovery potential is significantly constrained by operational conditions. When no nearby train is drawing power at the moment of braking, the regenerated energy cannot be reused and is instead dissipated as heat.

In traditional diode-based traction substations (TSSs), regenerative braking energy cannot be fed back to the grid, and power flows only from the substation to the train. As a result, when no nearby train is consuming power, the regenerated energy is dissipated as heat, even when scheduling strategies are used to align braking and traction phases [7,8]. Energy storage systems (ESSs) have been explored to mitigate this problem [9], including flywheels [10], batteries [11,12], and supercapacitors [13,14], deployed either onboard or wayside [15,16]. However, ESSs suffer from finite capacity, high cost, space and maintenance constraints, and strong dependence on train density and operating patterns, making them insufficient as standalone solutions. Reversible traction substations (RTSSs) address these limitations by enabling two-way power flow between trains and the grid, allowing surplus RBE to be exported rather than wasted. Recent studies have investigated RTSS designs using antiparallel inverters or controlled rectifier structures [17], with various implementation approaches reviewed in [18,19].

To contextualize the role of RTSS among existing energy-saving strategies, Table 1 compares RTSS, stationary ESS, and timetable optimization across key performance criteria. Studies show that ESS typically provides moderate energy-recovery improvements in the range of 12–32%, but its effectiveness is restricted by state-of-charge limitations, installation costs, and strong dependence on traffic density [20,21]. Timetable optimization yields only modest gains (4–15%) and is effective primarily when braking and traction phases can be synchronized along the timetable [22–24]. In contrast, RTSS achieves more consistent and generally higher recovery rates (10–40%) because surplus regenerative energy can always be exported to the grid, regardless of train spacing or operating patterns [25,26]. Beyond energy-recovery efficiency, RTSS also offers higher scalability across feeder sections and lower long-term maintenance demands compared with storage-based alternatives. While ESS and timetable adjustments remain useful in specific contexts—particularly in dense metro systems—this comparison highlights RTSS as a more flexible and cost-effective solution for large-scale, mixed-traffic DC railway networks.

The use of PWM rectifiers in railway traction substations has been shown to offer clear advantages over traditional diode or thyristor rectifiers, including higher efficiency, improved power quality, faster dynamic response, and greater flexibility [27,28]. These benefits make PWM-based RTSS architectures strong candidates for modernizing aging DC railway infrastructure. However, accurately predicting their impact is challenging because railway systems exhibit strong coupling between trains, substations, and the grid. High-fidelity models capable of reproducing realistic dynamic conditions are therefore essential.

Hardware-in-the-Loop (HIL) platforms have become increasingly important for validating converter behavior and control strategies before deployment [29], supporting the development of scalable solutions needed to meet future sustainability and energy-efficiency goals. Existing modeling approaches span steady-state power-flow analysis [30] to dynamic simulation frameworks [31], while real-time HIL provides the ability to capture fast converter transients and interact with hardware. Nevertheless, many studies rely on simplified converter or train models, and power-quality behavior under realistic multi-event RTSS operation remains insufficiently examined. Meanwhile, in all of these literature, transient-state modeling, and steady-state modeling are carried out separately and exclusively [32].

Table 1. Comparison of key energy-saving strategies for regenerative braking energy utilization.

Category	RTSS	ESS	Timetable Optimization
Energy Recovery Efficiency	10–40% depending on traffic and grid receptivity [25,26]	12–32% according to [20,21]	4–15% improvement depending on headway [22–24]
Dependence on Train Density/Scheduling	Low, energy can always be exported to grid	High, limited by SOC and traffic density	Very High, requires overlapping braking/traction trains
Scalability	High, benefits entire feeder section	Medium, localized at installation site	Low–Medium constrained by operational rules
Investment Cost	Medium–High	High, due to storage and PCS costs	Very Low
Maintenance Needs	Moderate (power electronics)	High, aging of batteries and SC	Minimal
Applicable Scenarios	Mixed-traffic lines, long headways, strong grid	Dense metro, high braking frequency	Metro lines with flexible dwell times

In light of this, the paper presents a DT-oriented real-time modeling and evaluation framework for a bilateral DC railway system with RTSS, incorporating both system-level and converter-level studies. This approach enables the physical system to provide real data, such as line data, train positions, traffic conditions, and so on, while also estimating transient events and power-quality issues and analyzing peak powers and voltage drops. Several substation attributes and loading situations are evaluated using the current network data of the Italian 3 kV DC railway line as a real-world case study to identify the optimal design while considering crucial performance metrics. Moreover, an experimental validation is performed using an HIL setup with OPAL-RT, allowing real-time testing of converter and system-level dynamics under realistic operational conditions. The DT concept is adopted from a design-stage perspective, where a detailed virtual model of the RTSS, including the DC feeder, train dynamics, and converter-level controls, is executed in real time and coupled with laboratory hardware through HIL. This DT-oriented modeling approach enables realistic emulation of train movements, power-quality phenomena, and bidirectional energy flow, providing a validated virtual environment that can serve as the core of a future operational digital twin when connected to live measurements from the railway network.

The paper develops as follows in the next sections: the working principles of the bilateral ERS under study with RTSS are explained in Section 2. Section 3 then explores the proposed modeling and control approach. In Section 4, extensive case study-based simulations are conducted, complemented by the HIL-based experimental results. The paper's closing remarks are summarized in Section 5.

2. Principles of the System Under Study

Figure 1 depicts the overall layout of the bilateral 3 kV ERS under investigation. It consists of segments that are connected by a shunt connection of two identical TPSSs and are used as a bilateral power supply for the DC railway line. The overhead catenary line (OCL), trains, RTSS, and primary-side HV are the key structural components.

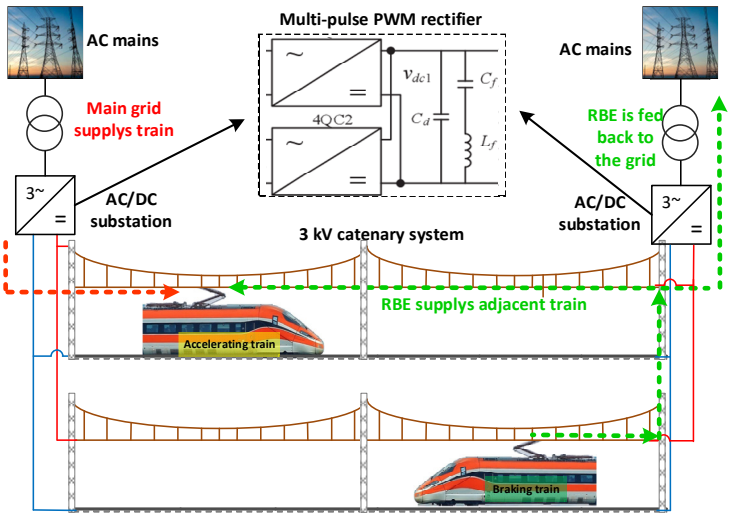

Figure 1. General configuration of the bilateral 3 kV railway system under study.

2.1. Modeling of RTSS with Primary-Side High-Voltage Grid

Multi-pulse TDRs, with an average of 15 km between each TPSS, are used in the current AC/DC conversion system in Italian 3 kV DC ERSs. Therefore, assuming that PWM rectifiers are used in place of conventional AC/DC conversion, the installation of the suggested RTSS is taken into consideration in the same position. The primary-side AC grid in the Italian suburban area, which is mostly based on 132 kV high voltage (HV), is connected to the projected RTSSs. Even though the voltage level and short length allow for a solely RL series line model, the line capacitance is taken into account using a T-model.

At the TPSS, a multi-pulse step-down transformer with a zigzag primary-side connection is installed to modify the grid voltage for the conversion procedure. A distinct PWM rectifier based on the three-level neutral point-clamped (3L-NPC) type, which functions as a four-quadrant converter (4QC), is supplied by each secondary winding. Secondary-side Y connections have a phase shift of 15°. In RTSS locations, the nominal line voltage is 3.6 kV, with a 20% overvoltage potential because of relevant ERS norms. In the meantime, 2.4 kV is the minimum operating voltage.

The primary-side AC voltage must be lower than the DC-side voltage for a PWM converter to operate properly. As a result, the transformers' secondary-side voltage is adjusted to 1.7 kV. The power range of the current TPSS is used to size all RTSS PWM converters, and a 5.4 MW is in line with the typical nominal powers seen in Italian AC/DC conversion groups. At the 4QCs output, DC-link capacitors are used to reduce and even out the output DC voltage ripples. Moreover, inductor branches are placed upstream of every converter to support the rectifier's linear functioning. This is predicated on the possibility that the transformer's series inductance would not be sufficient to charge the DC-link capacitor at a higher voltage.

2.2. Modeling of Overhead Catenary Lines (OCL)

Over time, the overhead contact line (OCL) used in Italian 3 kV DC systems has undergone several upgrades to support higher speeds and increased traffic. As shown in Table 2, earlier designs employed two 100 mm^2 contact wires and a 120 mm^2 messenger wire [33], whereas modern configurations use larger cross sections and higher mechanical tensions to ensure stable pantograph–catenary interaction at speeds up to 250 km/h. For modeling purposes, the OCL and return track are represented as an equivalent series resistance and inductance, capturing their aggregate electrical behavior in the traction power supply system.

Table 2. Standard features of a 3 kV DC ERS OCL conductor [33].

Characteristics of Railway Lines		Contact Line		Messenger Wires		Contact Wires		
Maximum Speed (km/h)	Intensity of Traffic	Contact Line Copper Wire Section (mm^2)	Messenger Wires Number	Messenger Wires Section (mm^2)	Messenger Wires Mechanical Tension (N)	Contact Wires Number	Contact Wires Section (mm^2)	Contact Wires Mechanical Tension (N)
200	Low	320	1	120	1375	2	100	1000
200	Mean	440	2	120	1125	2	100	1000
200	High	610	2	155	1000	2	150	1125
250	Mean	540	2	120	1500	2	150	1875
250	High	610	2	155	1625	2	150	1875

In addition to accurately representing DC transient voltage events, the inductance is included to address possible interference that the contact line may cause to adjacent equipment. An EMU shunt capacitor of 1 mF is carefully calculated into the equation, building on the methods described in [34]. In series with an inductance, the contact line resistance and the track resistance (which acts as the back current's return conductor) are combined to form variable resistance. The difference in electrical resistance between trains and nearby passenger stations is depicted in Figure 2. It has been regarded as both up- and down-track. As seen in (1) and (2), the real-time values for each resistance vary according to the trains' positions.

$$\begin{cases} R_{1P} = R_b \times d_{T2P} \\ R_{2P} = R_b \times (d_{T1P} - d_{T2P}) \\ R_{3P} = R_b \times (L - d_{T1P}) \end{cases} \quad (1)$$

$$\begin{cases} R_{1D} = R_b \times d_{T2D} \\ R_{2D} = R_b \times (d_{T1D} - d_{T2D}) \\ R_{3D} = R_b \times (L - d_{T1D}) \end{cases} \quad (2)$$

where index P is dedicated to upper track parameters and D is dedicated to down track parameters. Per-unit length values of 0.0568 Ω/km and 1.3 mH/km are used to represent the contact line resistance and inductance.

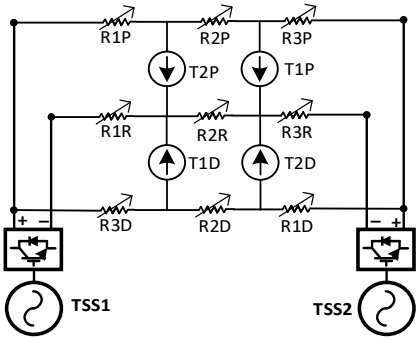

Figure 2. Modeling of OCL considering the electrical configuration of trains moving between two nearby TSS with varying resistances.

2.3. Modeling of Train Movements

To accurately represent the electrical load seen by the RTSS, the dynamic behavior of the train must be modeled, since traction and braking forces directly determine the current drawn from or injected into the DC network. The train model, therefore, includes the main mechanical forces acting on the vehicle and their influence on acceleration, braking, and

power demand. These elements form the basis for deriving the motion equations used in the simulation.

In the considered system, the traction transient current slope is limited to 22 kA/s, and the traction-to-brake dynamic slope is limited to 12 kA/s. To accurately model the dynamic behavior of the trains and assess the substation control strategy, all relevant forces must be considered, including gradients, resistance, tractive effort, and the traction effort–speed characteristic. Newton's second law and a full integration of these variables allow for the formulation of the equation defining the train's motion as follows:

$$\sum T = T_{Tr} - T_{Gr} - T_{Dr} = M_e \times a \tag{3}$$

In this case, a indicates the train's acceleration and Me its equivalent mass. The drag force (T_{Dr}), which is calculated using the Davis equation and information from train specifications, is essential for determining the load torque, whereas the tractive effort (T_{Tr}) includes the total tractive force:

$$T_{Dr} = a + bv_t + cv_t{}^2 \tag{4}$$

Furthermore, the forces generated by curves and gradients can be calculated as follows:

$$T_{Gr} = M_e \times g \times \sin\theta \tag{5}$$

The following formula is used to calculate the train's power based on its velocity and total force, where Paux represents the auxiliary internal power used and η_t represents the train's efficiency:

$$P_T = \frac{T \times v_t}{\eta_t} + P_{aux} \tag{6}$$

3. Proposed Model and Control System

In this work, the PWM-based voltage-oriented control (VOC) method was used as the modulation technique for regulating each 3L-NPC rectifier of the RTSS. This choice was made in light of the 3L converters' two-way characteristics and the goal of running at a power factor around 1 with few current harmonics. Over the past few decades, a variety of methods for controlling PWM rectifiers have been developed. These methods can be broadly divided into four categories: virtual-flux-oriented control, voltage-oriented control, voltage-based direct power control, and their combination. A common technique in power electronics for regulating the voltage and current of AC-DC converters and vice versa, such as in PWM rectifiers and inverters, is VOC [35–37]. The basic idea of VOC is to regulate the AC-side voltages' (or currents') amplitude and phase angle to guarantee the DC-side performance characteristics that are sought, including minimizing harmonic distortion and reaching unity power factor. The control approach in VOC is usually applied in a revolving reference frame (dq-frame) that is in line with the voltage of the AC supply. This makes the control design simpler by enabling the control system to separate the control of active (actual) power from reactive power. In order to control the output voltage or current in accordance with the reference values established by the control algorithm, the modulation technique employed in VOC modifies the switching signals of the power switches [38].

The ability of VOC to precisely adjust the output voltage or current while preserving high efficiency and good dynamic responsiveness is one of its main benefits. Applying the KVL for each NPC converter and decoupling the voltages and currents into their

respective dq components, then converting the input signals to an $\alpha\beta$ frame is modelled by the following equation:

$$\begin{pmatrix} V_{cd} \\ V_{cq} \end{pmatrix} = \begin{pmatrix} -(L_g s + R_g) & L_g\omega \\ -L_g\omega & -(L_g s + R_g) \end{pmatrix} \begin{pmatrix} i_d \\ i_q \end{pmatrix} + \begin{pmatrix} V_{gd} \\ V_{gq} \end{pmatrix} \quad (7)$$

While the other segments contain feed-forward terms intended to divide the control loops and improve overall capabilities, the initial components are controlled by a PI controller. Depending on the particular dynamic response needs, these terms may come from the reference values or the actual sensors. The total control approach is shown in Figure 3, where the angle ωt is determined using a PLL block that can monitor the network frequency when needed by following the steps described in Equation (7). The total current upstream of the inductances is the network current measured for controlling four 3L-NPC rectifiers, and the PWM modulation produces a total of 12 output pulses. As previously stated, the feed-forward components are carefully incorporated to support PI regulation. Since any noise would alter the control voltages, using real amounts rather than reference values assumes that these signals are comparatively noise-free. As an alternative, the measurements can be filtered to reduce noise, although this adds a delay that could cause performance to suffer during intense transients.

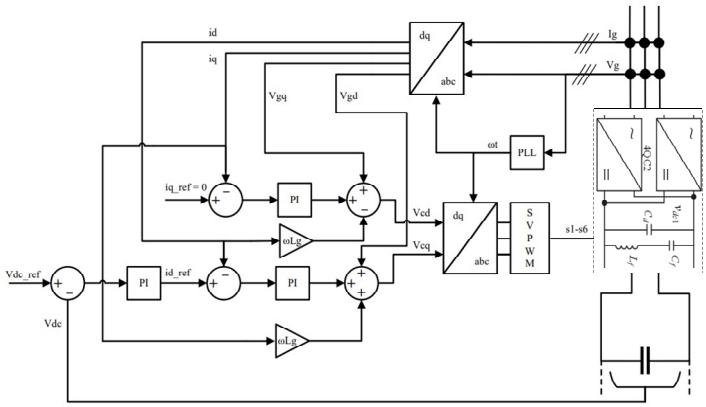

Figure 3. The suggested VOC-based approach for the proposed multi-pulse PWM rectifier.

To regulate the DC-link voltage (Vdc), the VOC's outer loop sets the d-axis current reference (id_ref), while setting the q-axis current reference (iq_ref) to zero eliminates reactive power exchange.

$$id\_ref = k_{p\_v}(V_{dc\_ref} - V_{dc}) + k_{i\_v}\int (V_{dc\_ref} - V_{dc})dt \quad (8)$$

The VOC inner current loops enforce regulation of the active and reactive currents to their reference values (id_ref, iq_ref). By decoupling the d- and q-axis dynamics, the control system achieves independent management of active and reactive power.

$$V_{d\prime} = k_{p\_i}(i_{d\_ref} - i_d) + k_{i\_i}\int (i_{d\_ref} - i_d)dt - \omega L i_q + v_d \quad (9)$$

$$V_{q\prime} = k_{p\_i}(i_{q\_ref} - i_q) + k_{i\_i}\int (i_{q\_ref} - i_q)dt - \omega L i_d + v_q \quad (10)$$

To better reflect the operating characteristics of DC railway systems, the VOC design used for the 3L-NPC converters in the RTSS is extended beyond the standard textbook formulation. The fast and discontinuous load variations caused by multiple trains accelerating or regenerating require explicit tuning of the VOC loops based on the AC-side converter

dynamics and the DC-link behavior of the 3 kV line. The AC-side of each NPC converter can be expressed in the synchronous dq frame as:

$$L_g \frac{di_d}{dt} = v_d - e_d + \omega L_g i_q - R_g i_d \tag{11}$$

$$L_g \frac{di_q}{dt} = v_q - e_q - \omega L_g i_d - R_g i_q \tag{12}$$

where

- L_g: grid-side inductance
- R_g: grid-side resistance
- e_d, e_q: grid voltages in dq frame
- ω: grid angular frequency

These equations illustrate the first-order nature of current dynamics and the cross-coupling terms $\omega L_g i_q$ and $\omega L_g i_d$, which are compensated through feed-forward components. Assuming perfect decoupling, the d-axis dynamics reduce to:

$$G_i(s) = \frac{i_d(s)}{v'_d(s)} \approx \frac{1}{L_g s + R_g} \tag{13}$$

Given the rapid current changes produced by traction and regenerative braking, the current-loop bandwidth $\omega_{c,i}$ can be selected to be 5–10 times the grid frequency, ensuring tracking of fast transients.

Considering the PI controller in (9) and (10), $G_{PI,i}(s) = k_{p_i} + \frac{k_{i_i}}{s}$, the gains can be tuned as:

$$k_{p_i} = L_g\, \omega_{c,i}, \qquad k_{i_i} = \alpha\, L_g\, \omega_{c,i}^2 \tag{14}$$

with $\alpha \in [0.2, 0.5]$ selected using the symmetrical-optimum criterion.

The DC-link dynamics are described by:

$$C_{dc} \frac{dV_{dc}}{dt} = i_{\text{conv}} - i_{\text{rail}} \tag{15}$$

where i_{conv} stands for the RTSS converter current and i_{rail} is the net railway load current (traction/braking sum).

The outer voltage PI controller in (7) $G_{PI,v}(s) = k_{p_v} + \frac{k_{i_v}}{s}$, can be tuned with bandwidth $\omega_{c,v} \approx \omega_{c,i}/10$:

$$k_{p_v} = C_{dc}\, \omega_{c,v},\ k_{i_v} = \beta\, C_{dc}\, \omega_{c,v}^2 \tag{16}$$

with β chosen to achieve the desired damping. Railway systems require load-dependent tuning because the converter is subjected to disturbances and very fast current steps.

4. Simulation Results

MATLAB/Simulink 2024b is used for the thorough analysis and implementation of the proposed railway network, which uses a PWM-based RTSS with a VOC. Detailed simulation parameters are shown in Table 3. The simulations cover a locomotive's whole traction cycle, including the acceleration, cruising, and braking phases, as illustrated in Figure 4a, in order to accurately evaluate the TSS performance under real-world circumstances. A normal timetable has been considered based on Figure 4b, which shows the possibility of train positions in the considered 15 km. Accordingly, two trains (one in the up track and one in the down track) are considered. A 15 km distance between TSSs is simulated while taking various loading and train location scenarios into account. Variable resistance that changes according to the position of trains is used to accurately replicate time-varying

OCL resistance. The analysis's primary objective is to assess RTSS performance from the perspective of power-quality issues using interleaved 3L-NPC converters. The high-speed train's power consumption on this route is assumed to be a maximum of 7.2 MW in acceleration mode. Because of the line restrictions, the train's top speed on this route is considered to be 150 km/h.

Table 3. Modeling and simulation parameters.

Simulated Parameter	Amount	Simulated Parameter	Amount
Primary voltage	132 kV	Contact line resistance	0.057 Ω/km
Network frequency	50 Hz	Contact line inductor	1.3 mH
Line resistance	0.17 Ω	Switching frequency	5000 Hz
Line inductance	0.63 mH	Nominal train power	7.2 MW
Traction transformer secondary voltage	1.72 kV	Traction transformer power	2 × 5.4 MW
DC-link capacitors	2 × 50 mF	Sampling time	10 µs
$k_{p\ VOC}$	0.016	$k_{i\ VOC}$	1
$k_{p\ DC\text{-}link}$	1.2	$k_{i\ VOC}$	25

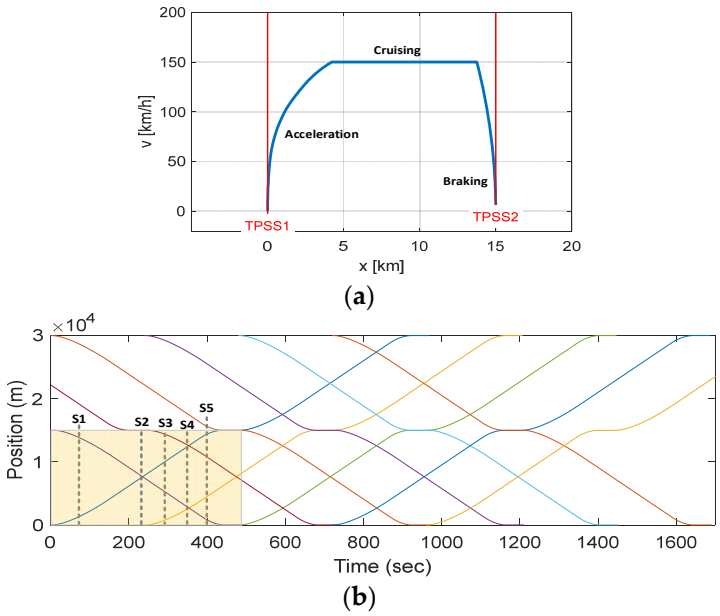

Figure 4. Primary data for the proposed system. (**a**) Simulated traction cycle. (**b**) Considered train timetable.

The pantograph voltage of the trains in both up-track and down-track configurations for both conventional and contemporary TPSSs is displayed in Figure 5. Whereas TPSS 2 is located at 15 km, TPSS 1 is presumed to be at 0 km. It is clear from Figure 5a that chopper switching and onboard rheostat energy waste cause the pantograph voltages to fluctuate significantly when in braking mode. The line voltage for a modern RTSS-based case is maintained with little variation between 3300 and 3750 V. Figure 6's profile of TPSS voltages demonstrates that, for RTSS, the voltage is maintained at a nominal value of 3600 V, but for TPSS with diodes (TDR-based TSS), the voltage fluctuates more. Particularly, the acceleration and braking phases of trains close to the substations are linked to the locations where the voltage drops and increases the most.

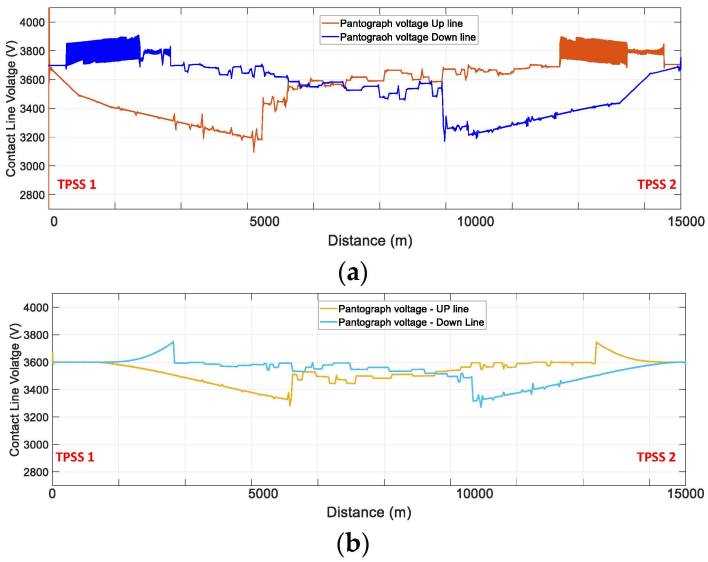

Figure 5. Pantograph voltages. (**a**) With TDR-based TPSS. (**b**) With new proposed RTSS.

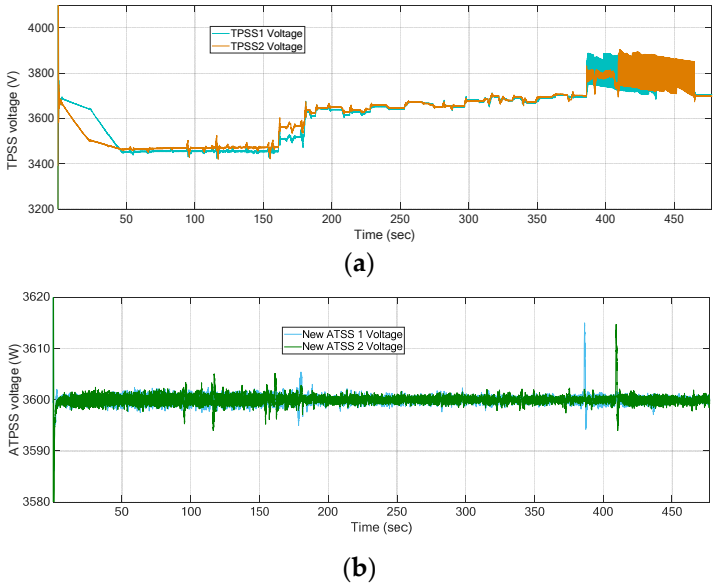

Figure 6. Traction substation voltages. (**a**) With traditional diode-bridge-based TPSS. (**b**) With RTSS.

The improved voltage profile observed in the RTSS case can be attributed to the PWM-based four-quadrant converters, which actively regulate the DC-link voltage and maintain a controlled power exchange with the AC grid. Unlike diode-based rectifiers, which respond passively to load variations, the RTSS continuously injects or absorbs power to stabilize the line voltage during acceleration and braking events. This active regulation reduces the large voltage dips and rises typically seen in traditional substations, particularly when trains operate close to the feeding point. The interleaved structure of the 3L-NPC converters further smooths the output current and reduces ripple, contributing to the more stable pantograph voltage.

The three-phase current of TPSS 1 for both traditional TSS and new RTSS are shown in Figure 7, together with the two traction and braking phases' fast Fourier transform (FFT) analysis. Although the current amplitude clearly varies during the braking, cruising, and acceleration phases, pulse and harmonic characteristics are present throughout all cycles.

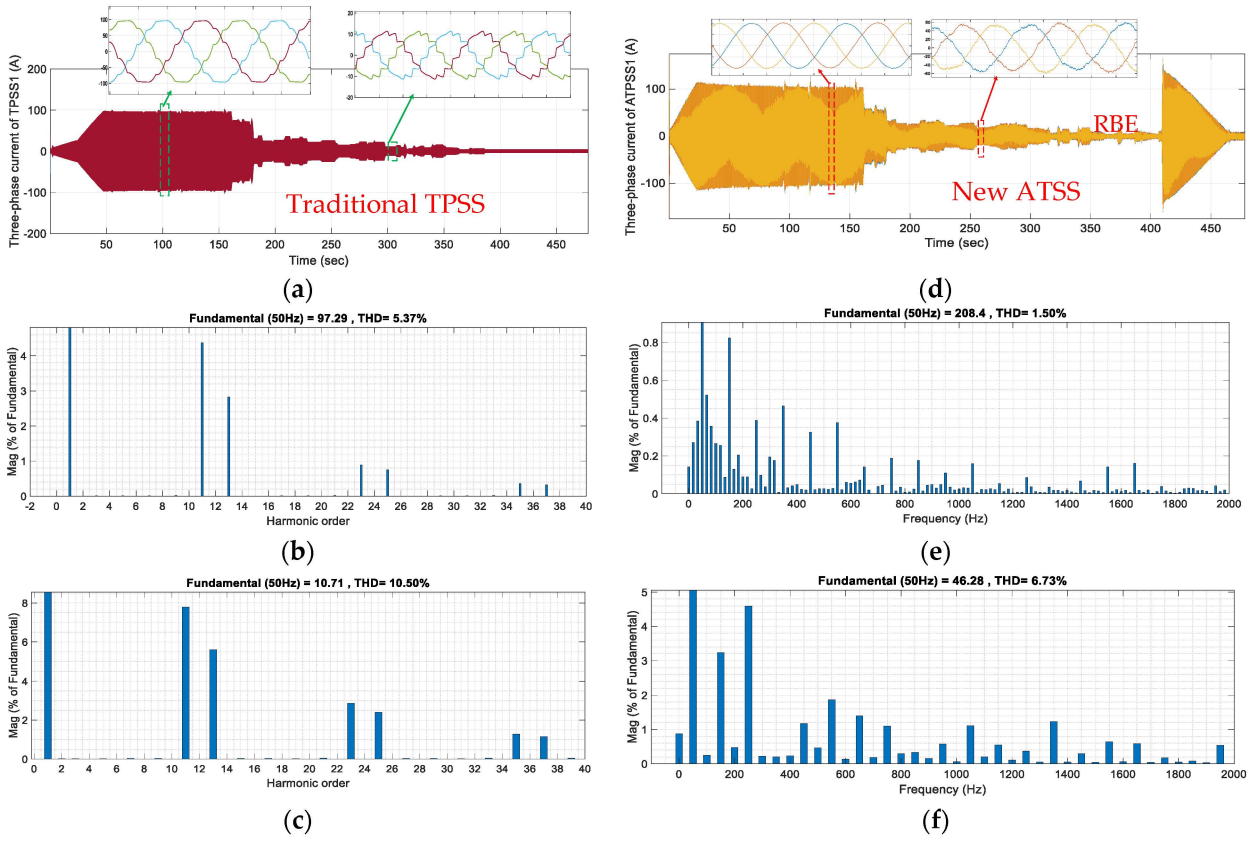

Figure 7. Primary-side currents of TDR-based TPSS and RTSS. (**a**) Three-phase currents for TDR-based TPSS; (**b**) FFT analysis for high current TDR-based TPSS; (**c**) FFT analysis for low current TDR-based TPSS. (**d**) Three-phase currents—new RTSS; (**e**) FFT analysis for high current—new RTSS; (**f**) FFT analysis for low current—new RTSS.

As shown in Figure 7b,c, for traditional TSS, total harmonic distortion (THD) increases by an average of 5.37% for larger currents and about 10.5% for lower currents due to the higher levels of the 11th and 13th low-order harmonics. Figure 7d–f shows the three-phase current and its FFT analysis for the suggested modern RTSS1. The current amplitude clearly spikes during braking periods as well. The currents are almost sinusoidal in nature. Figure 7e,f show a comparison of lower levels of low-order harmonics, which leads to an average drop in THD of 1.5% for larger currents and over 6.7% for lower currents. In comparison with traditional TSSs, new RTSSs show better power quality performance.

Overall, the harmonic behavior in Figure 7 also reflects the advantages of the proposed RTSS architecture. In traditional TSSs, the diode rectifier produces strong low-order harmonics (notably the 11th and 13th), which become more pronounced at lower load levels and result in higher THD. In contrast, the interleaved 3L-NPC converters used in the RTSS distribute the switching events among multiple parallel legs, effectively increasing the equivalent pulse number and canceling a portion of the lower-order harmonics. The multi-level modulation generates a staircase-type voltage waveform with smaller voltage steps, reducing dv/dt and improving current quality. As a result, the RTSS achieves visibly more sinusoidal currents and significantly lower THD in both high-load and low-load conditions. These effects also improve transformer utilization and reduce electromagnetic stress on upstream components.

5. Hardware-in-the-Loop (HIL) Based Experimental Results

In order to confirm the simulation results and validate the returning current to the grid from the train, the experimental setup features two programmable, bidirectional converters: a 6 kW unit and a high-power 72 kW unit, as shown in Figure 8. Each converter was installed on a designated test bench within the laboratory and equipped with the necessary measurement and monitoring tools for real-time data acquisition and analysis. In the proposed setup, the 6 kW converter acts as a train unit that can operate in both energy-consuming and energy-generating modes. This prototype includes regenerative braking capability, where the converter switches to generating power, mirroring how trains return energy to the grid during braking events. The two converters are connected via a shared DC link, enabling the low-power converter's absorbed power to be transferred to the high-power converter, which functions as the reversible traction substation. The high-power converter subsequently delivers this power to the grid, managing active and reactive power exchanges and ensuring AC-side voltage and current stability.

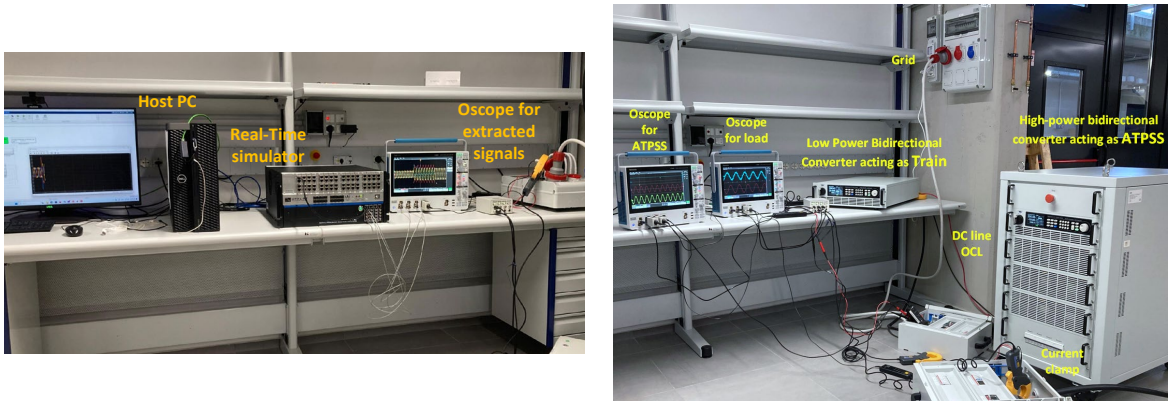

(**a**) (**b**)

Figure 8. Experimental setup of the proposed system, showing (**a**) the real-time simulator and (**b**) the bidirectional converters installed on laboratory test benches, forming the core of the DT-oriented real-time modeling and HIL platform.

To further validate and extend the laboratory results, a real-time HIL-based experimental validation setup was developed using the OPAL-RT 5707XG real-time platform, shown in Figure 8. The HIL setup reproduces the dynamic interaction between the emulated train converter and the RTSS under realistic grid conditions, enabling precise validation of control algorithms and power-flow management. Through the OPAL-RT environment, the simulated grid and converter models are executed in real time, while actual control signals and measurements are exchanged between the physical converters and the simulator. This configuration allows the assessment of bidirectional power flow, system stability, and regenerative braking performance under various operating scenarios. Although the HIL platform is used here strictly as an experimental validation tool, the real-time virtual model and its physical–virtual interfacing form the technical foundation for future digital twin development, as they provide the high-fidelity, real-time executable virtual asset required for DT-oriented analysis. The integrated HIL framework therefore ensures that the proposed system's energy-recovery and power-quality characteristics are accurately represented and validated both numerically and experimentally, while also supporting future extension toward digital twin applications. Although the laboratory experiment uses converters rated at 6 kW and 72 kW, it is important to emphasize that the HIL platform reproduces all power-system components, including traction transformers, feeders, and train loads, at their full megawatt-level ratings. In the OPAL-RT 5707XG real-time simulator, the entire

3 kV DC railway system is modeled in RT-Lab 2024/Simulink using the actual parameters and scales of the real Italian network, and the model executes with a fixed real-time step.

Figure 9 illustrates the measured phase voltage (c1) and current (c2) of the 72 kW converter acting as RTSS. The sinusoidal current waveform demonstrates the converter's effective performance, even under low-load conditions. It shows the capability of the proposed system and control method to feed back the RBE to the grid within an acceptable power-quality range. According to the power-quality analysis performed using the Tektronix oscilloscope, the 6 kW converter, acting as a train, absorbs approximately 800 Var with a power factor of around 0.72, while the 72 kW converter, acting as RTSS, compensates it and injects the RBE with a power factor close to −1. Figure 9 confirms this accuracy, where the nearly 180-degree phase shift between the voltage and current confirms a power factor close to −1, indicating the successful transfer of power back to the grid.

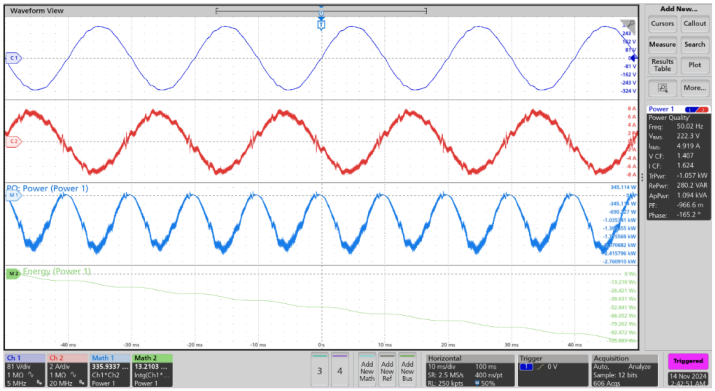

Figure 9. Experimental setup results. Measured phase voltage (c1) and current (c2) of the 72 kW converter acting as RTSS.

In order to validate the performance of the proposed system from a harmonic point of view, FFT analysis has been performed. Figures 10 and 11 illustrate the FFT analysis and THD% of the voltage and current waveforms of the converter under the studied load conditions. In Figure 10, the voltage FFT analysis reveals that the harmonic content is primarily concentrated at discrete frequencies corresponding to the switching characteristics of the converter. The logarithmic representation effectively highlights the relative amplitudes of higher-order harmonics, which diminish significantly as the frequency increases. Despite this reduction, the measured THD% of the voltage is approximately 6%, indicating the presence of some distortion. This level of distortion is expected under nominal operating conditions and is within acceptable limits for voltage waveforms in converter systems. In Figure 10, the FFT analysis shows that the current has a higher harmonic content compared to the voltage, with a current THD% of approximately 14%. This elevated THD% is primarily due to the lower load scenario considered in this study, which is a result of the power limitations of the lab converters used in the experimental setup. At lower load conditions, the relative impact of the harmonic components becomes more pronounced, leading to a higher current THD%. As the power range increases, the THD% of the current is expected to decrease, as the fundamental component of the current will dominate, reducing the relative contribution of harmonics. This behavior underscores the importance of evaluating harmonic distortion across different operating conditions to fully understand the system's performance and ensure compliance with power-quality standards.

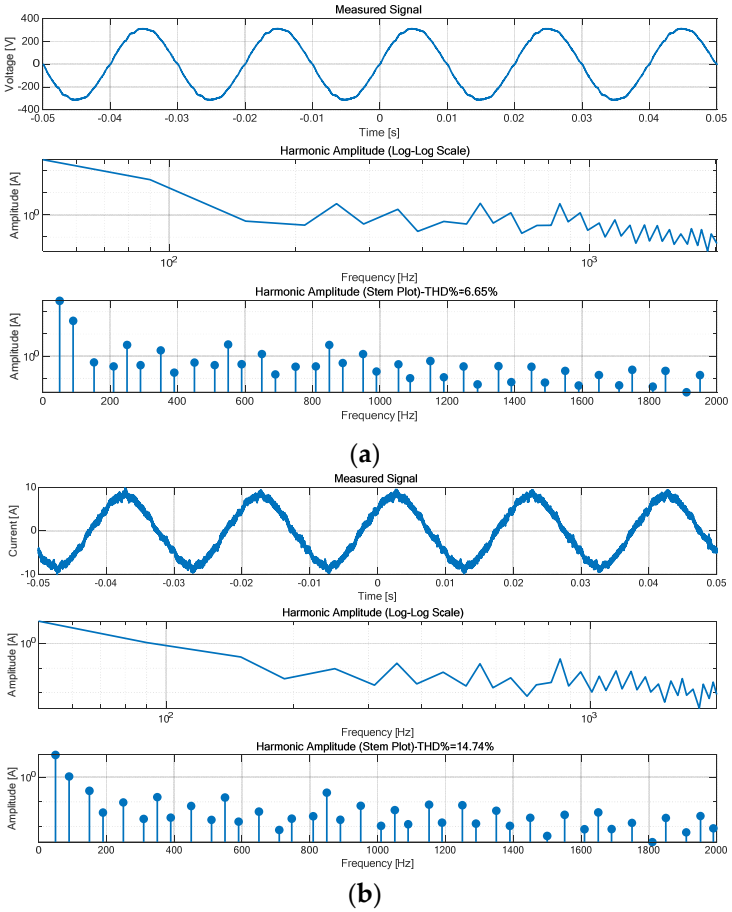

Figure 10. FFT analysis and THD% calculation. (**a**) For the converter's voltage. (**b**) For the converter's current.

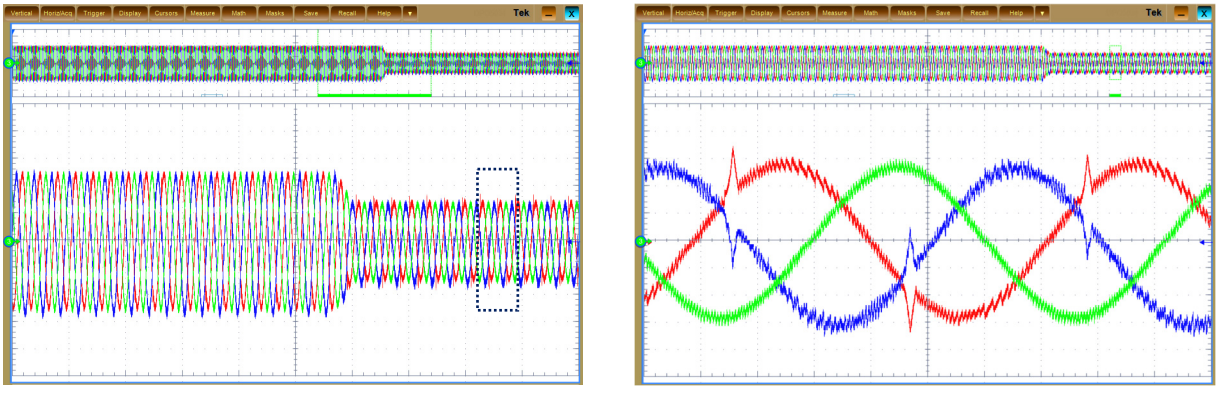

(**a**) (**b**)

Figure 11. The absorbed current in a real-time HIL simulation. (**a**) The ATSS current during changing load and dynamic conditions. (**b**) Zoomed area for 2 cycles.

Figure 11 presents the absorbed current waveforms obtained from the real-time HIL simulation of the proposed active traction substation (ATSS) during dynamic operating conditions. This figure plays a key role in validating the transient response and adaptability of the ATSS control strategy when subjected to variable load scenarios representative of real railway operation, where trains continuously change their power demand due to acceleration, coasting, and regenerative braking events.

In Figure 11a, the current waveform illustrates the ATSS's response to a sequence of load variations. These variations emulate the fluctuating power exchange between the traction network and the grid, mimicking a realistic operational profile of multiple

trains connected to the same feeder. The figure demonstrates that the ATSS is capable of maintaining a stable and well-regulated current profile even when the load conditions change abruptly. During these transitions, the converter adjusts its operation between power absorption and power injection modes, confirming the bidirectional functionality of the proposed system. This dynamic adaptability ensures that the system can effectively manage both motoring and braking phases of trains while maintaining grid stability and complying with power-quality standards.

Moreover, the waveform in Figure 11a exhibits a smooth transition between different operating states, with no evidence of significant overshoot or oscillations. This highlights the effectiveness of the implemented control algorithm, which dynamically regulates the current reference and ensures fast convergence to steady-state conditions. The control strategy employed in the ATSS thus demonstrates a strong ability to respond rapidly to dynamic load changes, which is essential in railway applications where the electrical demand can vary on a millisecond timescale.

Figure 11b provides a zoomed-in view of two cycles of the absorbed current, emphasizing the waveform quality and harmonic content during the transient event. The detailed representation confirms that the current waveform maintains a nearly sinusoidal shape with minimal distortion, even under dynamic operating conditions. This characteristic reflects the efficiency of the modulation technique and the robustness of the current control loop implemented in the converter. The absence of high-frequency oscillations or irregularities further indicates that the proposed ATSS control system effectively mitigates the impact of switching harmonics and maintains good synchronization with the grid voltage.

The results presented in Figure 11, combined with the FFT and THD analyses shown previously in Figure 10a,b, demonstrate that the ATSS can sustain high-quality current waveforms not only in steady-state operation but also under transient and dynamically varying load conditions. This performance confirms the suitability of the proposed converter topology and control method for real railway applications, where reliable bidirectional power flow and high-quality current waveforms are essential. In summary, the analysis of Figure 11 validates the real-time performance of the system, proving that the ATSS can effectively handle power exchanges between the railway traction network and the grid, ensuring operational flexibility, power quality, and system stability in both steady-state and transient conditions.

To assess the consistency between the numerical MATLAB/Simulink-based model and the experimental HIL setup, the key dynamic responses, such as current settling time, voltage regulation, harmonic content, and power-flow transitions, were directly compared with the corresponding simulation results. Although the hardware converters operate at reduced kW ratings, the OPAL-RT real-time model executes the full MW-scale railway system using the exact parameters of the simulated network. As a result, the transient shapes, steady-state behavior, and power-quality indicators observed in HIL closely match those obtained in the simulation. The small deviations that appear in the measured waveforms are mainly attributed to unavoidable laboratory non-idealities, such as sensor noise, switching dead times, and the finite bandwidth of the physical filters, rather than inaccuracies in the digital model. These deviations remain within acceptable engineering limits and confirm that the proposed RTSS control and system dynamics are faithfully represented in both the MATLAB/Simulink simulations and the real-time HIL validation.

6. Conclusions

The advantages of reversible traction substations equipped with interleaved PWM rectifiers for enhancing the utilization of regenerative braking energy in bilateral railway

lines have been comprehensively investigated in this study. Using the Italian 3 kV DC railway system as a case study, the proposed 4QC-based RTSS architecture featuring interleaved 3L-NPC converters and zigzag transformers was analyzed against traditional diode-bridge TPSS using a full traction cycle model to capture dynamic train behavior with high fidelity.

Simulation results show that the proposed RTSS significantly improves OCL voltage regulation, reduces passive-component stress, lowers primary-side harmonic distortion, and enhances power factor during both traction and braking phases. The RTSS also demonstrates an improved capability to recover and reinject regenerative braking energy into the grid with high power quality.

The HIL validation further confirms these findings, demonstrating stable voltage profiles, rapid dynamic response, and low current and voltage distortion under variable load conditions. The real-time model–based control strategy achieves smooth transitions between operating modes and accurately reproduces expected RTSS behavior. While the present HIL platform operates at reduced hardware power levels, the OPAL-RT real-time simulation emulates all MW-scale components of the railway system, allowing meaningful evaluation of system-level performance.

Limitations of this study include the reduced laboratory converter ratings, which restrict the range of achievable operating points, and the use of an aggregated OCL representation that does not capture all spatial electromagnetic phenomena. Additionally, the present work focuses on technical validation and does not address economic assessment or large-scale deployment considerations.

Future work will extend the developed platform toward an operational digital twin by integrating real-time field data, enabling online monitoring, predictive assessment, and model-based optimization of RTSS in service. Further investigations will consider more detailed OCL electromagnetic models, multi-train coordination strategies, techno-economic optimization of RTSS sizing, and evaluation of deployment scenarios across larger sections of the railway network.

Overall, the combined simulation and HIL results demonstrate that the proposed RTSS architecture offers substantial improvements over traditional TPSS in terms of energy efficiency, power quality, and system stability, and provides a validated foundation for future DT-enabled monitoring and optimization of DC railway systems.

Author Contributions: In preparation of this paper, H.J.K. conducted the methodology, data curation, software-based simulations, experimental and HIL platform development, and writing—original draft, and M.B. and D.Z. conducted the validation, visualization, and resources and funding acquisition, along with editing and supervision. All authors have read and agreed to the published version of the manuscript.

Funding: This research was conducted under the auspices of MOST—Sustainable Mobility National Research Center and was supported by funding from the European Union NextGenerationEU (Piano Nazionale di Ripresa e Resilienza (PNRR)–Missione 4 Componente 2, Investimento 1.4—D.D. 1033 17/06/2022, CN00000023). The content of this manuscript represents the views and opinions of the authors alone; the European Union and the European Commission bear no responsibility for its contents.

Institutional Review Board Statement: Not applicable.

Informed Consent Statement: Not applicable.

Data Availability Statement: The data presented in this study are available on request from the corresponding author. The data are not publicly available due to privacy.

Conflicts of Interest: The authors declare no conflicts of interest.

Abbreviations

3L-NPC	Three-Level Neutral Point-Clamped Converter
4QC	Four-Quadrant Converter
DT	Digital Twin
ESS	Energy Storage System
FFT	Fast Fourier Transform
HIL	Hardware-in-the-Loop
Me	Equivalent Train Mass
OCL	Overhead Catenary Line
OCS	Overhead Contact System
PF	Power Factor
RBE	Regenerative Braking Energy
RTSS	Reversible Traction Substation
TDr	Drag Force (Davis Equation)
THD	Total Harmonic Distortion
TSS	Traction Substation System
TTr	Tractive Effort
TPSS	Traditional/PWM Traction Substation System
TDR	Traditional Diode-Based Rectifier
Vdc	DC-link Voltage of Converter
VOC	Voltage-Oriented Control
idref, iqref	d- and q-Axis Current References
PWM	Pulse Width Modulation

References

1. Hooijschuur, E.; den Elzen, M.G.; Dafnomilis, I.; van Vuuren, D.P. Analysis of cost-effective reduction pathways for major emitting countries to achieve the Paris Agreement climate goal. *Glob. Environ. Change Adv.* **2025**, *4*, 100014. [CrossRef]
2. Teng, X.; Lu, L.C.; Chiu, Y.H. How the European Union reaches the target of CO_2 emissions under the Paris Agreement. *Eur. Plan. Stud.* **2020**, *28*, 1836–1857. [CrossRef]
3. Kaleybar, H.J.; Brenna, M.; Zaninelli, D. Multi-pulse Active Substation for Power Quality Improvement and Recuperation of Regenerative Braking Energy in DC Railway. In Proceedings of the 2024 21st International Conference on Harmonics and Quality of Power (ICHQP), Chengdu, China, 15–18 October 2024; pp. 37–42. [CrossRef]
4. Frilli, A.; Meli, E.; Nocciolini, D.; Pugi, L.; Rindi, A. Energetic optimization of regenerative braking for high speed railway systems. *Energy Convers. Manag.* **2016**, *129*, 200–215. [CrossRef]
5. Jiang, Y.; Liu, J.; Tian, W.; Shahidehpour, M.; Krishnamurthy, M. Energy harvesting for the electrification of railway stations: Getting a charge from the regenerative braking of trains. *IEEE Electrif. Mag.* **2014**, *2*, 39–48. [CrossRef]
6. Khodaparastan, M.; Mohamed, A.A.; Brandauer, W. Recuperation of Regenerative Braking Energy in Electric Rail Transit Systems. *IEEE Trans. Intell. Transp. Syst.* **2019**, *20*, 2831–2847. [CrossRef]
7. Wang, P.; Bešinović, N.; Goverde, R.M.P.; Corman, F. Improving the Utilization of Regenerative Energy and Shaving Power Peaks by Railway Timetable Adjustment. *IEEE Trans. Intell. Transp. Syst.* **2022**, *23*, 15742–15754. [CrossRef]
8. Liu, H.; Zhou, M.; Guo, X.; Zhang, Z.; Ning, B.; Tang, T. Timetable Optimization for Regenerative Energy Utilization in Subway Systems. *IEEE Trans. Intell. Transp. Syst.* **2019**, *20*, 3247–3257. [CrossRef]
9. Yoshida, Y.; Figueroa, H.P.; Dougal, R.A. Comparison of energy storage configurations in railway microgrids. In Proceedings of the 2017 IEEE Second International Conference on DC Microgrids (ICDCM), Nuremburg, Germany, 27–29 June 2017; pp. 133–138. [CrossRef]
10. Gee, A.M.; Dunn, R.W. Analysis of Trackside Flywheel Energy Storage in Light Rail Systems. *IEEE Trans. Veh. Technol.* **2015**, *64*, 3858–3869. [CrossRef]
11. Jafari Kaleybar, H.; Golnargesi, M.; Brenna, M.; Zaninelli, D. Hybrid Energy Storage System Taking Advantage of Electric Vehicle Batteries for Recovering Regenerative Braking Energy in Railway Station. *Energies* **2023**, *16*, 5117. [CrossRef]
12. Kong, D.; Miyatake, M. Cooperative Application of Onboard Energy Storage and Stationary Energy Storage in Rail Transit Based on Genetic Algorithm. *Energies* **2024**, *17*, 1426. [CrossRef]

13. Cui, G.; Luo, L.; Liang, C.; Hu, S.; Li, Y.; Cao, Y.; Xie, B.; Xu, J.; Zhang, Z.; Liu, Y.; et al. Supercapacitor integrated railway static power conditioner for regenerative braking energy recycling and power quality improvement of high-speed railway system. *IEEE Trans. Transp. Electrif.* **2019**, *5*, 702–714. [CrossRef]
14. Gabaldon, A.; Ruiz-Abellon, M.C.; Martinez, F.; Guillamón, A. Demand Management in Hybrid Locomotives Through Aggregated Models of Supercapacitors and Railway Units. *Appl. Sci.* **2025**, *15*, 2412. [CrossRef]
15. Saeed, M.; Briz, F.; Guerrero, J.M.; Larrazabal, I.; Ortega, D.; Lopez, V.; Valera, J.J. Onboard energy storage systems for railway: Present and trends. *IEEE Open J. Ind. Appl.* **2023**, *4*, 238–259. [CrossRef]
16. Liu, X.; Li, K. Energy storage devices in electrified railway systems: A review. *Transp. Saf. Environ.* **2020**, *2*, 183–201. [CrossRef]
17. Kleftakis, V.A.; Hatziargyriou, N.D. Optimal Control of Reversible Substations and Wayside Storage Devices for Voltage Stabilization and Energy Savings in Metro Railway Networks. *IEEE Trans. Transp. Electrif.* **2019**, *5*, 515–523. [CrossRef]
18. Kaleybar, H.J.; Brenna, M.; Pugi, L. Reversible Traction Substations in DC Railway Systems: A Comparative Study of Approaches. In Proceedings of the 2023 IEEE International Conference on Environment and Electrical Engineering and 2023 IEEE Industrial and Commercial Power Systems Europe (EEEIC/I&CPS Europe), Madrid, Spain, 6–9 June 2023; pp. 1–6. [CrossRef]
19. Imran, M.S.; Amjad, Q.A. Analytical Analysis of 3kV DC Railway Regenerative Braking Energy Storage System with Current Controlled DC-DC Bidirectional Converters. Master's Thesis, ING-School of Industrial and Information Engineering, Milano, Italy, 2017.
20. Ceraolo, M.; Lutzemberger, G.; Meli, E.; Pugi, L.; Rindi, A.; Pancari, G. Energy Storage Systems to Exploit Regenerative Braking in DC Railway Systems: Different Approaches to Improve Efficiency of Modern High-Speed Trains. *J. Energy Storage* **2018**, *16*, 269–279. [CrossRef]
21. Arboleya, P.; Bidaguren, P.; Armendariz, U. Energy Is on Board: Energy Storage and Other Alternatives in Modern Light Railways. *IEEE Electr. Mag.* **2016**, *4*, 30–41. [CrossRef]
22. Zhao, N.; Tian, Z.; Hillmansen, S.; Chen, L.; Roberts, C.; Gao, S. Timetable Optimization and Trial Test for Regenerative Braking Energy Utilization in Rapid Transit Systems. *Energies* **2022**, *15*, 4879. [CrossRef]
23. Chen, W.; Lu, J.; Zhang, H.; Yuan, Z. Pareto Optimization of Energy-Saving Timetables Considering the Non-Parallel Operation of Multiple Trains on a Metro Line. *Mathematics* **2023**, *11*, 4491. [CrossRef]
24. Yang, X.; Li, X.; Ning, B.; Tang, T. A Survey on Energy-Efficient Train Operation for Urban Rail Transit. *IEEE Trans. Intell. Transp. Syst.* **2016**, *17*, 2–13. [CrossRef]
25. Barrero, R.; Tackoen, X.; Van Mierlo, J. Stationary or Onboard Energy Storage Systems for Energy Consumption Reduction in a Metro Network. *Proc. Inst. Mech. Eng. Part F J. Rail Rapid Transit* **2010**, *224*, 207–225. [CrossRef]
26. Fan, Z.; Stewart, B.G. Power Flow Simulation of DC Railway Power Supply Systems with Reversible Substations. In Proceedings of the IEEE Mediterranean Electrotechnical Conference (MELECON 2020), Palermo, Italy, 16–18 June 2020.
27. Shimizu, T.; Fujita, T.; Kimura, G.; Hirose, J. A unity power factor PWM rectifier with DC ripple compensation. *IEEE Trans. Ind. Electron.* **1997**, *44*, 447–455. [CrossRef]
28. Rodríguez, J.R.; Dixon, J.W.; Espinoza, J.R.; Pontt, J.; Lezana, P. PWM regenerative rectifiers: State of the art. *IEEE Trans. Ind. Electron.* **2005**, *52*, 5–22. [CrossRef]
29. Zhang, G.; Tian, Z.; Tricoli, P.; Hillmansen, S.; Liu, Z. A new hybrid simulation integrating transient-state and steady-state models for the analysis of reversible dc traction power systems. *Int. J. Electr. Power Energy Syst.* **2019**, *109*, 9–19. [CrossRef]
30. Paul, F.-G.; Guerrero, J.M.; Muniategui-Aspiazu, I.; Vicente-Makazaga, I.; Endema, A.; Rodriguez, D.O.; Briz, F. Power-Hardware-in-the-Loop Emulation of the Low-Frequency Oscillation Phenomenon in AC Railway Networks. *IEEE Access* **2022**, *10*, 87374–87386. [CrossRef]
31. Herrero, M.M.; Mendez, A.R.; Caballo, I.C.; Aspiazu, I.M.; Arza, J. Hardware-in-the-Loop Platform for Virtual Certification of Traction Systems for Railway. *IEEE Access* **2024**, *12*, 52182–52194. [CrossRef]
32. Cheng, Y.; Liu, Z.; Huang, K. Transient analysis of electric arc burning at insulated rail joints in high-speed railway stations based on state-space modeling. *IEEE Trans. Transp. Electrif.* **2017**, *3*, 750–761. [CrossRef]
33. Kaleybar, H.J.; Brenna, M.; Foiadelli, F. Compatibility of Present 3 kV DC and 2 × 25 kV AC High-Speed Railway Power Supply Systems Towards Future MVDC System. In Proceedings of the 2021 12th Power Electronics, Drive Systems, and Technologies Conference (PEDSTC), Tabriz, Iran, 2–4 February 2021; pp. 1–6. [CrossRef]
34. Llaneza, M.G.; Kaleybar, H.J.; Brenna, M. Implementation of Active Power Substation for Harvesting Regenerative Braking Energy in Italian 3 kV Railway Systems. In Proceedings of the 2023 AEIT International Annual Conference (AEIT), Rome, Italy, 5–7 October 2023; pp. 1–6. [CrossRef]
35. Hasheminasab, S.; Alzayed, M.; Chaoui, H. A Review of Control Techniques for Inverter-Based Distributed Energy Resources Applications. *Energies* **2024**, *17*, 2940. [CrossRef]
36. Mahlooji, M.H.; Mohammadi, H.R.; Rahimi, M. A review on modeling and control of grid-connected photovoltaic inverters with LCL filter. *Renew. Sustain. Energy Rev.* **2018**, *81*, 563–578. [CrossRef]

37. Yan, S.; Yang, Y.; Hui, S.Y.; Blaabjerg, F. A review on direct power control of pulsewidth modulation converters. *IEEE Trans. Power Electron.* **2021**, *36*, 11984–12007. [CrossRef]
38. Hansen, S.; Malinowski, M.; Blaabjerg, F.; Kazmierkowski, M.P. Sensorless control strategies for PWM rectifier. In Proceedings of the APEC 2000, Fifteenth Annual IEEE Applied Power Electronics Conference and Exposition (Cat. No. 00CH37058), New Orleans, LA, USA, 6–10 February 2000; pp. 832–838.